AIAA JOURNAL
Vol. 42, No. 7, July 2004

Finite Element Analysis of Smart Structures Containing Piezoelectric Fiber-Reinforced Composite Actuator

M. C. Ray* and Nilanjan Mallik†
Indian Institute of Technology, Kharagpur 721 302, India

Static analysis of laminated smart composite plates integrated with a piezoelectric fiber-reinforced composite (PFRC) layer acting as distributed actuators has been carried out by a generalized-energy-based finite element model. A simple first-order shear deformation theory is used for deriving the model. Eight noded isoparametric serendipity elements are used for discretizing the domain. The performance of the PFRC layer has been investigated for both symmetric and antisymmetric cross-ply and antisymmetric angle-ply laminated composite shell substrates. The effect of piezoelectric fiber orientation on the control authority of the PFRC layer has also been studied.

Introduction

DURING the past decade, demand for piezoelectric materials as distributed sensors and/or actuators has been significantly increased for active control of vibration of high performing lightweight smart structures.[1–17] This demand is credited to their inherent property of direct (capability of inducing an electric potential/charge when subjected to a mechanical load) and converse (capability of being deformed due to the externally applied voltage/charge) piezoelectric effects. Flexible structures when coupled with a layer/patch of these materials acting as distributed sensor and/or actuator are customarily known as smart structures. Recently, piezoelectric materials have also been used to achieve active control of sound radiated from flexible structures.[18–20]

The control authority of the existing monolithic piezoelectric materials is very low because their piezoelectric stress/strain coefficients are of very small magnitudes. Tailoring of these piezoelectric coefficients may be the possible means to improve the control authority of piezoelectric materials. In an endeavor to tailor these piezoelectric properties, the authors[21] recently investigated the effective mechanical and piezoelectric properties of unidirectional piezoelectric fiber-reinforced composite (PFRC) materials. The main concern of the investigation was to determine the effective piezoelectric coefficient e_{31} of the PFRC materials that quantifies the induced normal stress in the fiber direction due to the applied electric field in the direction transverse to the fiber direction. It has been found that this effective piezoelectric coefficient becomes significantly larger than the corresponding coefficient of piezoelectric material of the fibers. Note that this piezoelectric coefficient is mainly responsible for active control of vibration of smart structures. In a previous paper, the authors[22] investigated the performance of a layer of this PFRC material as a distributed actuator for smart structures by use of the method of exact solutions. However, it is well known that the exact solutions are not possible for problems with complicated geometry and more general boundary and loading conditions. The finite element method has been firmly established as a most popular tool for solving such problems.

In this paper, the authors intend to develop a finite element model for static analysis of smart composite plates integrated with a layer of PFRC material acting as distributed actuators. The effect of fiber orientation in the PFRC layer should play an important role in the actuating capability of the PFRC layer and has been addressed in this study using this finite element model.

Received 22 July 2003; revision received 13 November 2003; accepted for publication 18 December 2003.

*Assistant Professor, Department of Mechanical Engineering; mcray@mech.iitkgp.ernet.in.
†Research Scholar, Department of Mechanical Engineering.

Finite Element Modeling

Figure 1 shows a simply supported rectangular laminated substrate plate made of N number of orthotropic layers. The length, width, and thickness of plate are denoted as a, b, and h, respectively. The top surface of the plate is integrated with a layer of the PFRC material, which acts as a distributed actuator of the plate. Figure 2 schematically presents the constructional feature of a lamina made of this PFRC material. The midplane of the substrate plate is considered as the reference plane. The origin of the laminate coordinate system x, y, z is located on the reference plane in such a way that $x = 0, a$ and $y = 0, b$ indicate the boundaries of the substrate plate. Also, the thickness coordinates z of the top and bottom surfaces of any kth layer are h_{k+1} and h_k, respectively. The axes of elastic symmetry in any layer kth of the overall plate are oriented at an angle θ_k with respect to the laminate coordinate system.

The displacement field for modeling the kinematics of deformations of the overall plate is based on the first-order shear deformation theory (FSDT) as

$$u(x, y, z) = u_0(x, y) + z\theta_x(x, y) \tag{1}$$

$$v(x, y, z) = v_0(x, y) + z\theta_y(x, y) \tag{2}$$

$$w(x, y, z) = w_0(x, y) \tag{3}$$

in which u, v, and w are the total mechanical displacements in the laminate space along the x, y, and z axes, respectively; u_0, v_0, and w_0 are the generalized displacements of a reference point (x, y) on the midplane $(z = 0)$ of the substrate along the x, y, and z axes, respectively; θ_x and θ_y are the generalized rotations of the normal to reference point on the reference plane $(z = 0)$ lying in the xz and yz planes, respectively. For the ease of analysis, the generalized displacement variables are separated into translational $\{d_t\}$ and rotational $\{d_r\}$ variables as follows:

$$\{d_t\} = [u_0 \quad v_0 \quad w_0]^T, \qquad \{d_r\} = [\theta_x \quad \theta_y]^T \tag{4}$$

The state of strain at a point in the overall plate is described by two vectors of in-plane strains $\{\epsilon_b\}$ and transverse shear strains $\{\epsilon_s\}$, respectively, and are given by

$$\{\epsilon_b\} = [\epsilon_x \quad \epsilon_y \quad \epsilon_{xy}]^T, \qquad \{\epsilon_s\} = [\epsilon_{xz} \quad \epsilon_{yz}]^T \tag{5}$$

When the linear strain/displacement relations and the displacement field given by Eqs. (1)–(3) are used, the in-plane strain vector $\{\epsilon_b\}$ and the transverse shear strain vector $\{\epsilon_s\}$ can be written as

$$\{\epsilon_b\} = \{\epsilon_{bt}\} + z\{\epsilon_{br}\}, \qquad \{\epsilon_s\} = \{\epsilon_{st}\} + [z]_s\{\epsilon_{sr}\} \tag{6}$$

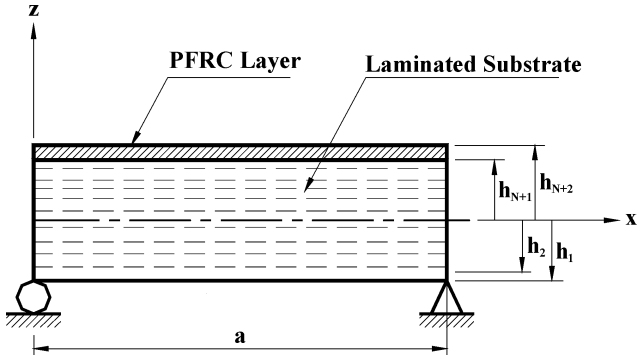

Fig. 1 Laminated composite substrate integrated with a PFRC layer.

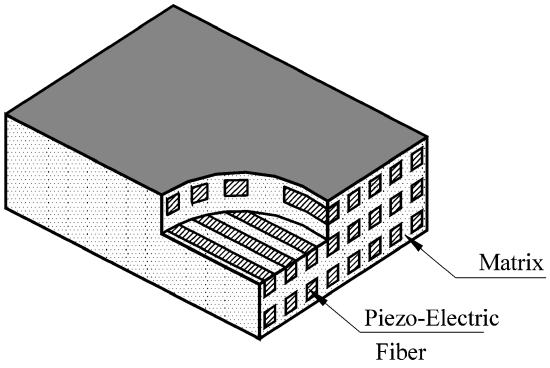

Fig. 2 Schematic diagram of a lamina of PFRC.

where the generalized strain vectors $\{\in_{bt}\}$, $\{\in_{br}\}$, $\{\in_{st}\}$, and $\{\in_{sr}\}$ are given by

$$\{\in_{bt}\} = \left[\frac{\partial u_0}{\partial x} \quad \frac{\partial v_0}{\partial y} \quad \frac{\partial u_0}{\partial y} + \frac{\partial v_0}{\partial x}\right]^T$$

$$\{\in_{br}\} = \left[\frac{\partial \theta_x}{\partial x} \quad \frac{\partial \theta_y}{\partial y} \quad \frac{\partial \theta_x}{\partial y} + \frac{\partial \theta_y}{\partial x}\right]^T$$

$$\{\in_{st}\} = \left[\frac{\partial w_0}{\partial x} \quad \frac{\partial w_0}{\partial y}\right]^T, \qquad \{\in_{sr}\} = [\theta_x \quad \theta_y]^T$$

$$[z]_s = \begin{bmatrix} 1 & 0 \\ 0 & 1 \end{bmatrix} \tag{7}$$

It is assumed that the surface of the PFRC layer being in contact with the substrate layer is suitably grounded. Because the thickness of the PFRC layer is very low, the variation of the electric potential function across the thickness may be considered as linear. Thus, the form of the electric potential function $\phi(x, y, z)$ can be expressed as[11]

$$\phi(x, y, z) = \frac{z - h_{N+1}}{h_{N+2} - h_{N+1}} \phi_0(x, y), \qquad h_{N+2} \le z \le h_{N+1} \tag{8}$$

where ϕ_0 is the generalized electric potential function similar to the generalized displacement functions at any point on the surface ($z = h_{N+2}$) of the PFRC actuator layer.

Similar to the strain vectors given by Eq. (5), the in-plane stresses and transverse shear stresses at any point in the overall plate are described by the following stress vectors:

$$\{\sigma_b\} = [\sigma_x \quad \sigma_y \quad \sigma_{xy}]^T, \qquad \{\sigma_s\} = [\sigma_{xz} \quad \sigma_{yz}]^T \tag{9}$$

where σ_x and σ_y are the normal stresses in x and y directions, respectively; σ_{xy} is the in-plane shear stress; and σ_{xz} and σ_{yz} are the transverse shear stresses.

The constitutive relations for the material of any layer kth of the overall plate considered in the present study can be expressed as

$$\left\{\sigma_b^k\right\} = \left[\bar{C}_b^k\right]\left\{\in_b^k\right\} - \left[\bar{e}_b^k\right]\{E^k\}, \qquad \left\{\sigma_s^k\right\} = \left[\bar{C}_s^k\right]\left\{\in_s^k\right\} - \left[\bar{e}_s^k\right]\{E^k\} \tag{10}$$

$$\{D^k\} = \left[\bar{e}_b^k\right]^T\left\{\in_b^k\right\} + \left[\bar{e}_s^k\right]^T\left\{\in_s^k\right\} + [\bar{\varepsilon}^k]\{E^k\} \tag{11}$$

where, for the kth layer, $[\bar{C}_b^k]$ and $[\bar{C}_s^k]$ are the matrices of transformed elastic coefficients referred to (x, y, z) coordinate systems; $[\bar{e}_b^k]$ and $[\bar{e}_s^k]$ are the matrices of corresponding transformed piezoelectric constants; $\{E^k\}$ and $\{D^k\}$ are the electric field and electric displacement vectors, respectively; and $[\bar{\varepsilon}^k]$ is the matrix of transformed dielectric constants. Here the electric field and displacement vectors appearing in Eqs. (10) and (11) are given by

$$\{E^k\} = \left[E_x^k \quad E_y^k \quad E_z^k\right]^T, \qquad \{D^k\} = \left[D_x^k \quad D_y^k \quad D_z^k\right]^T \tag{12}$$

in which E_x^k, E_y^k, and E_z^k are the electric field along the x, y, and z axes, respectively, and D_x^k, D_y^k, and D_z^k are the corresponding electric displacements. In Eqs. (10) and (11) the matrices $[\bar{C}_b^k]$, $[\bar{C}_s^k]$, $[\bar{e}_b^k]$, $[\bar{e}_s^k]$, and $[\bar{\varepsilon}^k]$ are given by[23]

$$\left[\bar{C}_b^k\right] = \begin{bmatrix} \bar{C}_{11}^k & \bar{C}_{12}^k & \bar{C}_{16}^k \\ \bar{C}_{21}^k & \bar{C}_{22}^k & \bar{C}_{26}^k \\ \bar{C}_{16}^k & \bar{C}_{26}^k & \bar{C}_{66}^k \end{bmatrix}, \qquad \left[\bar{C}_s^k\right] = \begin{bmatrix} \bar{C}_{55}^k & \bar{C}_{45}^k \\ \bar{C}_{45}^k & \bar{C}_{44}^k \end{bmatrix}$$

$$[\bar{e}_b^k] = \begin{bmatrix} 0 & 0 & \bar{e}_{31}^k \\ 0 & 0 & \bar{e}_{32}^k \\ 0 & 0 & \bar{e}_{36}^k \end{bmatrix}, \qquad \left[\bar{e}_s^k\right] = \begin{bmatrix} \bar{e}_{15}^k & \bar{e}_{25}^k & 0 \\ \bar{e}_{14}^k & \bar{e}_{24}^k & 0 \end{bmatrix}$$

$$[\bar{\varepsilon}^k] = \begin{bmatrix} \bar{\varepsilon}_{11}^k & \bar{\varepsilon}_{12}^k & 0 \\ \bar{\varepsilon}_{12}^k & \bar{\varepsilon}_{22}^k & 0 \\ 0 & 0 & \bar{\varepsilon}_{33}^k \end{bmatrix} \tag{13}$$

If the elastic, dielectric, and piezoelectric coefficients of the kth layer are known with respect to its material coordinate system, then the various elements of the given matrices can be derived from the work by Reddy.[23] Note here that, without the electrical terms, Eq. (10) represents the constitutive equations for each orthotropic layer of the laminated substrate.

The total potential energy of the plate coupled with the PFRC layer can be expressed as[11]

$$T_P = \frac{1}{2}\left[\sum_{k=1}^{N+1} \int_{\vartheta} \left(\left\{\in_b^k\right\}^T\left\{\sigma_b^k\right\} + \left\{\in_s^k\right\}^T\left\{\sigma_s^k\right\}\right) \mathrm{d}\vartheta \right.$$

$$\left. - \int_{\vartheta} \{E^{N+1}\}^T\{D^{N+1}\}\,\mathrm{d}\vartheta\right] - \int_A \{d\}^T\{f\}\,\mathrm{d}A \tag{14}$$

where $\{f\}$ is the externally applied surface traction vector acting over a surface area A and ϑ is the volume of the concerned domain.

The overall plate is discretized by eight noded isoparametric quadrilateral elements. When Eq. (4) is used, the generalized displacement vectors for the ith, $i = 1, 2, 3, \ldots, 8$, node of the element can be denoted as

$$\{d_{ti}\} = [u_{0i} \quad v_{0i} \quad w_{0i}]^T, \qquad \{d_{ri}\} = [\theta_{xi} \quad \theta_{yi}]^T \tag{15}$$

and the generalized displacement vectors at any point within the element can be written as

$$\{d_t\} = [N_t]\left\{d_t^e\right\}, \qquad \{d_r\} = [N_r]\left\{d_r^e\right\} \tag{16}$$

In Eq. (16), the nodal generalized translational displacement vector $\{d_t^e\}$, the nodal generalized rotational displacement vector $\{d_r^e\}$, and the shape function matrices $[N_t]$ and $[N_r]$ are given by

$$\begin{aligned}
\left\{d_t^e\right\} &= \begin{bmatrix}\{d_{t1}\}^T & \{d_{t2}\}^T & \cdots & \{d_{t8}\}^T\end{bmatrix}^T \\
\left\{d_r^e\right\} &= \begin{bmatrix}\{d_{r1}\}^T & \{d_{r2}\}^T & \cdots & \{d_{r8}\}^T\end{bmatrix}^T \\
[N_t] &= [N_{t1} \quad N_{t2} \quad \cdots \quad N_{t8}] \\
[N_r] &= [N_{r1} \quad N_{r2} \quad \cdots \quad N_{r8}] \\
N_{ti} &= n_i I_t, \qquad N_{ri} = n_i I_r
\end{aligned} \tag{17}$$

where I_t and I_r are the identity matrices and n_i is the shape function of natural coordinates associated with the node i. When the relations given by Eqs. (7) and (16) are used, the generalized strain vectors at any point within the element are obtained as

$$\begin{aligned}
\{\in_b\} &= [B_{tb}]\left\{d_t^e\right\} + z[B_{rb}]\left\{d_r^e\right\} \\
\{\in_s\} &= [B_{ts}]\left\{d_t^e\right\} + [z]_s[B_{rs}]\left\{d_r^e\right\}
\end{aligned} \tag{18}$$

In Eq. (18), the nodal generalized strain/displacement matrices $[B_{tb}]$, $[B_{rb}]$, $[B_{ts}]$, and $[B_{rs}]$ are given by

$$\begin{aligned}
[B_{tb}] &= [B_{tb1} \quad B_{tb2} \quad \cdots \quad B_{tb8}] \\
[B_{rb}] &= [B_{rb1} \quad B_{rb2} \quad \cdots \quad B_{rb8}] \\
[B_{ts}] &= [B_{ts1} \quad B_{ts2} \quad \cdots \quad B_{ts8}] \\
[B_{rs}] &= [B_{rs1} \quad B_{rs2} \quad \cdots \quad B_{rs8}]
\end{aligned} \tag{19}$$

The various submatrices in Eq. (19) can be found as follows:

$$[B_{tbi}] = \begin{bmatrix} \dfrac{\partial n_i}{\partial x} & 0 & 0 \\ 0 & \dfrac{\partial n_i}{\partial y} & 0 \\ \dfrac{\partial n_i}{\partial y} & \dfrac{\partial n_i}{\partial x} & 0 \end{bmatrix}, \qquad [B_{rbi}] = \begin{bmatrix} \dfrac{\partial n_i}{\partial x} & 0 \\ 0 & \dfrac{\partial n_i}{\partial y} \\ \dfrac{\partial n_i}{\partial y} & \dfrac{\partial n_i}{\partial x} \end{bmatrix}$$

$$[B_{tsi}] = \begin{bmatrix} 0 & 0 & \dfrac{\partial n_i}{\partial x} \\ 0 & 0 & \dfrac{\partial n_i}{\partial y} \end{bmatrix}, \qquad [B_{rsi}] = \begin{bmatrix} n_i & 0 \\ 0 & n_i \end{bmatrix} \tag{20}$$

In a similar manner, the generalized electric potential vector at any point within the element can be expressed as

$$\phi_0 = [N_\phi]\left\{\phi_0^e\right\} \tag{21}$$

where $\{\phi_0^e\} = [\phi_{01} \ \phi_{02} \ \cdots \ \phi_{08}]^T$ and $[N_\phi] = [n_1 \ n_2 \ \cdots \ n_8]$. When Eqs. (8), (12), and (21) and electric field-potential relations are used, the electric field vector can be expressed in terms of the nodal generalized electric potential degrees of freedom $\{\phi_0^e\}$ as follows:

$$\{E^k\} = [Z_p][B_p]\left\{\phi_0^e\right\} \tag{22}$$

in which $[B_p] = [B_{p1} \ B_{p2} \ \cdots \ B_{p8}]$ with

$$[B_{pi}] = \begin{bmatrix} \dfrac{\partial n_i}{\partial x} & \dfrac{\partial n_i}{\partial y} & n_i \end{bmatrix}^T$$

$$[Z_p] = \frac{1}{(h_{N+2} - h_{N+1})} \begin{bmatrix} -(z - h_{N+1}) & 0 & 0 \\ 0 & -(z - h_{N+1}) & 0 \\ 0 & 0 & -1 \end{bmatrix}$$

When Eqs. (10) and (11) are substituted into Eq. (14) and then Eqs. (18) and (22) are used, the total potential energy T_P^e of a typical element augmented with the PFRC layer can be expressed as

$$\begin{aligned}
T_P^e = \tfrac{1}{2}\Big[&\left\{d_t^e\right\}^T\left[K_t^e\right]\left\{d_t^e\right\} + \left\{d_t^e\right\}^T\left[K_{tr}^e\right]\left\{d_r^e\right\} + \left\{d_r^e\right\}^T\left[K_{rt}^e\right]\left\{d_t^e\right\} \\
&+ \left\{d_r^e\right\}^T\left[K_{rr}^e\right]\left\{d_r^e\right\} - \left\{d_t^e\right\}^T\left[F_{tp}^e\right]\left\{\phi_0^e\right\} - \left\{d_r^e\right\}^T\left[F_{rp}^e\right]\left\{\phi_0^e\right\} \\
&- \left\{\phi_0^e\right\}^T\left[F_{pt}^e\right]\left\{d_t^e\right\} - \left\{\phi_0^e\right\}^T\left[F_{pr}^e\right]\left\{d_r^e\right\} \\
&- \left\{\phi_0^e\right\}^T\left[K_D^e\right]\left\{\phi_0^e\right\}\Big] - \left\{d_t^e\right\}^T\{F^e\}
\end{aligned} \tag{23}$$

In Eq. (23), the elemental stiffness matrices $[K_t^e]$, $[K_{tr}^e]$, $[K_{rt}^e]$, and $[K_{rr}^e]$; the elemental electro-elastic coupling matrices $[F_{tp}^e]$, $[F_{rp}^e]$, $[F_{pt}^e]$, and $[F_{pr}^e]$; the elemental dielectric stiffness matrix $[K_D^e]$ and the elemental load vector $[\boldsymbol{F}^e]$ are defined as follows:

$$\left[K_t^e\right] = \left[K_{tb}^e\right] + \left[K_{ts}^e\right], \qquad \left[K_{tr}^e\right] = \left[K_{trb}^e\right] + \left[K_{trs}^e\right]$$

$$\left[K_{rr}^e\right] = \left[K_{rrb}^e\right] + \left[K_{rrs}^e\right], \qquad \left[K_{tr}^e\right] = \left[K_{tr}^e\right]^T$$

$$\left[K_{tb}^e\right] = \int_0^{b_e}\int_0^{a_e} [B_{tb}]^T[D_{tb}][B_{tb}]\,\mathrm{d}x\,\mathrm{d}y$$

$$\left[K_{ts}^e\right] = \int_0^{b_e}\int_0^{a_e} [B_{ts}]^T[D_{ts}][B_{ts}]\,\mathrm{d}x\,\mathrm{d}y$$

$$\left[K_{trb}^e\right] = \int_0^{b_e}\int_0^{a_e} [B_{tb}]^T[D_{trb}][B_{rb}]\,\mathrm{d}x\,\mathrm{d}y$$

$$\left[K_{trs}^e\right] = \int_0^{b_e}\int_0^{a_e} [B_{ts}]^T[D_{trs}][B_{rs}]\,\mathrm{d}x\,\mathrm{d}y$$

$$\left[K_{rrb}^e\right] = \int_0^{b_e}\int_0^{a_e} [B_{rb}]^T[D_{rrb}][B_{rb}]\,\mathrm{d}x\,\mathrm{d}y$$

$$\left[K_{rrs}^e\right] = \int_0^{b_e}\int_0^{a_e} [B_{rs}]^T[D_{rrs}][B_{rs}]\,\mathrm{d}x\,\mathrm{d}y$$

$$\left[\boldsymbol{F}_{tp}^e\right] = \int_0^{b_e}\int_0^{a_e} [B_{tb}]^T[D_{tp}][B_p]\,\mathrm{d}x\,\mathrm{d}y$$

$$\left[\boldsymbol{F}_{rp}^e\right] = \int_0^{b_e}\int_0^{a_e} [B_{rb}]^T[D_{rp}][B_p]\,\mathrm{d}x\,\mathrm{d}y, \qquad \left[\boldsymbol{F}_{pt}^e\right] = \left[\boldsymbol{F}_{tp}^e\right]^T$$

$$\left[\boldsymbol{F}_{pr}^e\right] = \left[\boldsymbol{F}_{rp}^e\right]^T, \qquad \left[K_D^e\right] = \int_0^{b_e}\int_0^{a_e} [B_p]^T[D_D][B_p]\,\mathrm{d}x\,\mathrm{d}y$$

$$\left[\boldsymbol{F}^e\right] = \int_0^{b_e}\int_0^{a_e} [N_t]^T\{f\}\,\mathrm{d}x\,\mathrm{d}y$$

where a_e and b_e are the length and width of the element in consideration and

$$[D_{tb}] = \sum_{k=1}^{N+1}\int_{h_k}^{h_{k+1}} \left[\bar{C}_b^k\right]\mathrm{d}z, \qquad [D_{ts}] = \sum_{k=1}^{N+1}\int_{h_k}^{h_{k+1}} \left[\bar{C}_s^k\right]\mathrm{d}z$$

$$[D_{trb}] = \sum_{k=1}^{N+1}\int_{h_k}^{h_{k+1}} z\left[\bar{C}_b^k\right]\mathrm{d}z$$

$$[D_{trs}] = \sum_{k=1}^{N+1}\int_{h_k}^{h_{k+1}} \left[\bar{C}_s^k\right][z]_s\,\mathrm{d}z$$

$$[D_{rrs}] = \sum_{k=1}^{N+1}\int_{h_k}^{h_{k+1}} [z]_s\left[\bar{C}_s^k\right][z]_s\,\mathrm{d}z$$

$$[D_{rrb}] = \sum_{k=1}^{N+1} \int_{h_k}^{h_{k+1}} z^2 \left[\bar{C}_b^k\right] \mathrm{d}z$$

$$[D_{tp}] = \int_{h_{N+1}}^{h_{N+2}} \left[\bar{e}_b^{N+1}\right][Z_p]\,\mathrm{d}z$$

$$[D_{rp}] = \int_{h_{N+1}}^{h_{N+2}} z\left[\bar{e}_b^{N+1}\right][Z_p]\,\mathrm{d}z$$

$$[D_D] = \int_{h_{N+1}}^{h_{N+2}} [Z_p]^T [\bar{\varepsilon}^{N+1}][Z_p]\,\mathrm{d}z$$

When the principle of minimum total potential energy, that is, $\delta T_P^e = 0$, is applied, the following governing equations of an element are obtained:

$$\left[K_t^e\right]\left\{d_t^e\right\} + \left[K_{tr}^e\right]\left\{d_r^e\right\} = \left[\boldsymbol{F}_{tp}^e\right]\left\{\phi_0^e\right\} + \{F^e\} \tag{24}$$

$$\left[K_{rt}^e\right]\left\{d_t^e\right\} + \left[K_{rr}^e\right]\left\{d_r^e\right\} = \left[\boldsymbol{F}_{rp}^e\right]\left\{\phi_0^e\right\} \tag{25}$$

Note here that to activate the PFRC layer, electric potential (voltage) will be specified at the top surface of the PFRC layer. Thus, $\delta\{\phi_0^e\}$ will be zero while yielding the preceding governing equations for the element.

When elemental governing equations are assembled into global space, the global equations of equilibrium are obtained as follows:

$$[K_t]\{X_t\} + [K_{tr}]\{X_r\} = [F_{tp}]\{\Phi\} + \{F\} \tag{26}$$

$$[K_{rt}]\{X_t\} + [K_{rr}]\{X_r\} = [F_{rp}]\{\Phi\} \tag{27}$$

where $[K_t]$, $[K_{tr}]$, and $[K_{rr}]$ are the global stiffness matrices; $[F_{tp}]$ and $[F_{rp}]$ are the global electroelastic coupling matrices; $\{X_t\}$ and $\{X_r\}$ are the global nodal generalized displacement vectors; $\{F\}$ is the global nodal mechanical force vector; and $\{\Phi\}$ is the global nodal electric potential vector. After the imposition of the displacement boundary conditions, the global rotational degrees of freedom can be condensed to obtain the global equilibrium equation in terms of global translational degrees of freedom only as follows:

$$[K]\{X_t\} = \left[F_{tp}^*\right]\{\Phi\} + \{F\} \tag{28}$$

in which $[K] = [K_t] - [K_{tr}][K_{rr}]^{-1}[K_{rt}]$ and $[F_{tp}^*] = [F_{tp}] - [K_{tr}][K_{rr}]^{-1}[F_{rp}]$. Equation (28) represents the electroelastic finite element model to assess the performance of the PFRC layer considered in this study. Also, note that, for implementing the selective integration rule in a straightforward manner, the stiffness matrices corresponding to bending and transverse shear deformations are derived separately to avoid shear locking in thin laminated substrates.

Numerical Results

In this section, the numerical results are evaluated using the finite element model derived in the preceding section. Both cross-ply and angle-ply substrates are considered for numerical examples. The thickness of each layer of all of the substrates is considered as 1 mm. The materials of the piezoelectric fiber and the matrix of the PFRC layer are PZT5H and epoxy, respectively. When a 40% fiber volume fraction is considered, the elastic and piezoelectric properties of the PFRC layer with respect to its material coordinate system are evaluated by the micromechanics model developed by the authors[21] and are presented in Tables 1 and 2, respectively. Table 1 also contains

Table 1 Elastic constants of the PFRC[21] and substrate layers[23]

Elastic constant	PFRC	Substrate layers
C_{11}, GPa	32.6	172.93
C_{12}, GPa	4.3	1.73
C_{22}, GPa	7.2	6.92
C_{44}, GPa	1.05	1.15
C_{55}, GPa	1.29	2.87
C_{66}, GPa	1.29	3.45

Table 2 Piezoelectric properties of the PFRC layer[21]

Property	Value
e_{31}, C/m^2	−6.76
ε_{11}, F/m	0.037×10^{-9}
ε_{22}, F/m	10.46×10^{-9}
ε_{33}, F/m	10.46×10^{-9}

Table 3 Response of symmetric cross-ply (0/90/0) square substrates with negligible thickness of PFRC layer

s	w^*	σ_x^*	σ_y^*	σ_{xy}^* [a]
10				
Present FEM	0.6690	0.5132	0.2531	0.0252
Analytical[23]	0.6693	0.5134	0.2536	0.0252
20				
Present FEM	0.4921	0.5317	0.1990	0.0223
Analytical[23]	0.4921	0.5318	0.1997	0.0223
100				
Present FEM	0.4336	0.5373	0.1796	0.0213
Analytical[23]	0.4337	0.5384	0.1804	0.0213

[a]Where $(\sigma_x^*, \sigma_y^*, \sigma_{xy}^*) = \max(\bar{\sigma}_x, \bar{\sigma}_y, \bar{\sigma}_{xy})$ and $w^* = \bar{w}(a/2, b/2, 0)$.

the material properties of the orthotropic layers of the substrates. It has been found from the micromechanical analysis[21] that the values of the other piezoelectric coefficients, e_{32}, e_{33}, e_{15}, and e_{24}, are much smaller than that of e_{31} and, hence, are not considered in the evaluation of the numerical results.

The results are evaluated with and without applying the electrical potential distribution on the actuator surface for different values of length to thickness ratio $s\ (= a/h)$. The following nondimensional parameters are used for presenting the numerical results:

$$\bar{u} = \frac{E_T u^k}{f_0 s^3 h}, \qquad \bar{w} = \frac{100 E_T w^k}{f_0 s^4 h}, \qquad \bar{\sigma}_x = \frac{\sigma_x^k}{f_0 s^2}$$

$$\bar{\sigma}_y = \frac{\sigma_y^k}{f_0 s^2}, \qquad \bar{\sigma}_{xy} = \frac{\sigma_{xy}^k}{f_0 s^2}$$

where f_0 is either the magnitude of amplitude of the sinusoidally distributed load or the magnitude of the intensity of the uniformly distributed load. The prescribed electric potential distribution on the surface, $z = h_{N+2}$, of the PFRC layer is considered either as spatially distributed sinusoidal electric potential or uniformly distributed electric potential with amplitude V (volt). Unless otherwise mentioned, the piezoelectric fiber orientation ψ in the PFRC layer is considered as 0 deg. The following simply supported boundary conditions are used for cross-ply substrates to evaluate the numerical results[23]:

$$v_0 = w = \theta_y = 0 \qquad \text{at} \qquad x = 0, a$$

$$u_0 = w = \theta_x = 0 \qquad \text{at} \qquad y = 0, b$$

whereas those for angle-ply substrates are considered as[23]

$$u_0 = w = \theta_y = 0 \qquad \text{at} \qquad x = 0, a$$

$$v_0 = w = \theta_x = 0 \qquad \text{at} \qquad y = 0, b$$

The comparison scheme followed for the validity of the present finite element model is to find the responses of the substrates integrated with an inactivated PFRC layer of negligible thickness and subsequently to compare these responses with the existing analytical responses[23] of the identical substrates without integrated with the PFRC layer.[23] Tables 3, 4, and 5 show such comparisons of responses for symmetric cross-ply, antisymmetric cross-ply, and antisymmetric angle-ply substrates, respectively. Note from Tables 3–5 that the responses are in excellent agreement.

Next, with the assumption that the thickness of the PFRC layer is 250 μm and the amplitude of distributed sinusoidal mechanical

load is $f_0 = 40$ N/m^2 (downward), the mechanical displacements u and w and in-plane stresses σ_x, σ_y, and σ_{xy} for symmetric and anti-symmetric cross-ply substrates are computed with and without applying the spatial sinusoidally distributed electric potential on the surface of the PFRC layer and are compared with the exact solutions derived by the authors.[22] These results are provided in Tables 6 and 7. Note from Tables 6 and 7 that the results for thin substrates match with high accuracy, whereas slight errors are observed for thick plate substrates, $s = 10$. The maximum percentage difference between the present finite element solutions and the exact solutions is observed to be 12.6% in case of computing the in-plane shear stress σ_{xy} for very thick antisymmetric cross-ply substrate. In Tables 3–5, it is shown that with negligible thickness of the PFRC layer the results are in excellent agreement with the analytical solutions[23] for both thick and thin plates using FSDT. Also, it is known that the FSDT underpredicts the deflections and stresses in comparison to the exact solutions[23] and is true for the present finite element solutions. Hence, these errors for thick substrate plates may be attributed to the use of FSDT and can be reduced to a great extent if one uses high-order shear deformation theory. At this point, note that the lightweight smart structures are usually very thin, and thus, the present finite element model can be reliably used for the analysis of such structures because the results for thin substrate plates are highly accurate.

Table 4 Response of antisymmetric cross-ply square substrates with negligible thickness of PFRC layer

	(0/90)			$(0/90)_4$		
s	w^*	σ_y^*	σ_{xy}^*	w^*	σ_y^*	$\sigma_{xy}^{*\,a}$
10						
Present FEM	1.2372	0.7154	0.0525	0.6199	0.4947	0.0221
Analytical[23]	1.2373	0.7157	0.0525	0.6216	0.4950	0.0221
20						
Present FEM	1.1073	0.7153	0.0525	0.4915	0.4947	0.0221
Analytical[23]	1.1070	0.7157	0.0525	0.4913	0.4950	0.0221
100						
Present FEM	1.0655	0.7123	0.0522	0.4495	0.4939	0.0221
Analytical[23]	1.0653	0.7157	0.0525	0.4496	0.4950	0.0221

[a]Where $(\sigma_x^*, \sigma_y^*, \sigma_{xy}^*) = \max(\bar{\sigma}_x, \bar{\sigma}_y, \bar{\sigma}_{xy})$ and $w^* = \bar{w}(a/2, b/2, 0)$.

Table 5 Response of antisymmetric angle-ply square substrates with negligible thickness of PFRC layer

	$(-45/45)_1$			$(-45/45)_4$		
Parameter	$s = 10$	$s = 20$	$s = 100$	$s = 10$	$s = 20$	$s = 100$
$w^{*\,a}$						
Present FEM	0.8281	0.6982	0.6566	0.4195	0.2895	0.2479
Analytical[23]	0.8284	0.6981	0.6564	0.4198	0.2896	0.2479
σ_x^*						
Present FEM	0.2468	0.2468	0.2468	0.1427	0.1427	0.1427
Analytical[23]	0.2498	0.2498	0.2498	0.1445	0.1445	0.1445
σ_{xy}^*						
Present FEM	0.2334	0.2334	0.2334	0.1384	0.1384	0.1384
Analytical[23]	0.2336	0.2336	0.2336	0.1384	0.1384	0.1384

[a]Where $(\sigma_x^*, \sigma_y^*, \sigma_{xy}^*) = \max(\bar{\sigma}_x, \bar{\sigma}_y, \bar{\sigma}_{xy})$ and $w^* = \bar{w}(a/2, b/2, 0)$.

Next, the responses for cross-ply and angle-ply substrates are computed using this finite element model (FEM) when the substrates are subjected to uniformly distributed mechanical load ($f_0 = -40$ N/m^2) and the PFRC layer is activated with uniformly distributed electric potential on its surface. Tables 8, 9, and 10 contain these responses for thick and thin symmetric cross-ply (0/90/0), antisymmetric cross-ply (0/90/0/90), and antisymmetric angle-ply (−45/45/−45/45) substrates, respectively.

An important aspect of developing this FEM is to investigate the effect of variation of fiber orientation ψ in the PFRC layer on its capability of actuating the laminated substrates. Figure 3 shows this effect of variation of the piezoelectric fiber orientation ψ in the PFRC layer on the center deflection of cross-ply laminated substrates. To use a criterion for determining the fiber orientation in the PFRC layer for which its control authority becomes maximum, a prescribed uniformly distributed electric potential is considered on the surface of the PFRC layer such that the resultant deflection becomes opposite to that caused by the uniformly distributed mechanical load alone acting vertically downward only. Thus, the greater is the resultant deflection under the combined action of mechanical and electrical load, the greater will be the control authority of the activated PFRC layer. Note from Fig. 3 that for symmetric cross-ply plate (0/90/0) the actuation capability of the PFRC layer is maximum when $\psi = 0$ deg. In the case of antisymmetric laminated plates

Table 6 Response of symmetric cross-ply square substrates (0/90/0) with and without applied voltage to the PFRC layer

	$s = 10$			$s = 20$			$s = 100$		
Method[a]	$V = 0$	$V = 100$	$V = -100$	$V = 0$	$V = 100$	$V = -100$	$V = 0$	$V = 100$	$V = -100$
Present FEM									
u^*	0.0058	−2.8204	2.8319	0.0060	−0.6929	0.7049	0.0061	−0.0217	0.0339
u^*	−0.0061	0.9246	−0.9368	−0.0064	0.2187	−0.2314	−0.0065	0.0024	−0.0153
Exact solution[22]									
u^*	0.0066	−3.141	3.1542	0.0063	−0.7229	0.7356	0.0062	−0.0223	0.0346
u^*	−0.0070	0.8897	−0.9038	−0.0067	0.2213	−0.2346	−0.0065	0.0026	−0.0157
Present FEM									
w^*	−0.6511	122.46	−124.7	−0.4571	28.287	−29.201	−0.4022	0.7632	−1.5776
Exact solution[22]									
w^*	−0.7100	132.9	−134.3	−0.4866	30.337	−31.31	−0.4089	0.7873	−1.6051
Present FEM									
σ_x^*	−0.4915	235.46	−236.4	−0.5022	57.267	−58.276	−0.4941	1.7483	−2.7364
σ_x^*	0.5215	−71.565	72.570	0.5304	−17.09	18.074	0.5121	0.2106	1.2478
Exact solution[22]									
σ_x^*	−0.5281	248.76	−249.8	−0.5035	57.269	−58.276	0.4948	1.7549	−2.7445
σ_x^*	0.5623	−71.666	72.79	0.5305	−17.81	18.875	0.5193	0.2181	1.2566
Present FEM									
σ_y^*	−0.2348	34.175	−34.645	−0.1849	9.888	−10.258	−0.1641	0.2571	−0.5807
σ_y^*	0.2573	−51.295	51.809	0.2040	−14.125	14.529	0.1707	−0.3926	0.7428
Exact solution[22]									
σ_y^*	−0.2571	42.532	−43.046	−0.1901	10.459	−10.84	−0.1643	0.2596	−0.5882
σ_y^*	0.2799	−57.667	58.227	0.2044	−14.16	14.566	0.1758	−0.3955	0.7470
Present FEM									
σ_{xy}^*	0.0241	−7.0066	7.0547	0.0214	−1.814	1.8565	0.0197	−0.0526	0.0915
σ_{xy}^*	−0.0251	4.2419	−4.292	−0.0224	1.1232	−1.1679	−0.0204	0.02502	−0.0658
Exact solution[22]									
σ_{xy}^*	0.0261	−7.696	7.748	0.0215	−1.822	1.8648	0.0197	−0.0527	0.0922
σ_{xy}^*	−0.0276	4.619	−4.674	−0.0224	1.1232	−1.1679	−0.0204	0.02506	−0.06596

[a]Where $u^* = \bar{u}(0, b/2, \pm h/2)$, $w^* = \bar{w}(a/2, b/2, 0)$, $\sigma_x^* = \bar{\sigma}_x(a/2, b/2, \pm h/2)$, $\sigma_y^* = \bar{\sigma}_y(a/2, b/2, \pm h/6)$, and $\sigma_{xy}^* = \bar{\sigma}_{xy}(0, 0, \pm h/2)$.

Table 7 Response of antisymmetric cross-ply square substrates (0/90/0/90) with and without applied voltage to the PFRC layer

	$s=10$			$s=20$			$s=100$		
Method[a]	$V=0$	$V=100$	$V=-100$	$V=0$	$V=100$	$V=-100$	$V=0$	$V=100$	$V=-100$
Present FEM									
u^*	0.0092	−4.5364	4.5643	0.0089	−0.8558	0.8735	0.0089	−0.0242	0.0419
u^*	−0.0059	0.9335	−0.9452	−0.0059	0.1626	−0.1744	−0.0059	0.0179	−0.0115
Exact solution[22]									
u^*	0.0104	−5.1094	5.1301	0.0094	−0.9500	0.9687	0.0090	−0.0248	0.0428
u^*	−0.0063	0.7755	−0.7882	−0.0060	0.1574	−0.1694	−0.0059	0.0183	−0.0118
Present FEM									
w^*	−0.6643	131.97	−131.68	−0.5102	30.142	−31.163	−0.4694	0.7584	−1.697
Exact solution[22]									
w^*	−0.7137	147.75	−149.17	−0.5351	32.383	−33.453	−0.4764	0.7818	−1.7346
Present FEM									
σ_x^*	−0.0360	14.981	−14.949	−0.0341	3.1082	−3.1765	−0.0328	0.0843	−0.1493
σ_x^*	0.4925	−61.683	62.853	0.4806	−12.850	13.740	0.4715	−0.0104	0.9524
Exact solution[22]									
σ_x^*	−0.0400	17.047	−17.127	−0.0347	3.2563	−3.3256	−0.0328	0.0849	−0.1506
σ_x^*	0.5079	−62.945	63.961	0.4810	−12.869	13.831	0.4720	−0.0110	0.9550
Present FEM									
σ_y^*	−0.0103	2.7947	−2.8135	−0.0103	0.7762	−0.7962	−0.0102	0.0225	−0.0429
σ_y^*	0.4641	−94.179	95.107	0.4426	−27.428	28.649	0.4351	−0.7489	1.6213
Exact solution[22]									
σ_y^*	−0.0103	2.8055	−2.8261	−0.0103	0.7772	−0.7977	−0.0102	0.0228	−0.0433
σ_y^*	0.4665	−100.95	101.89	0.4436	−27.857	28.744	0.4358	−0.7517	1.6232
Present FEM									
σ_{xy}^*	0.0236	−8.6436	8.6707	0.0237	−1.9451	1.9924	0.0230	−0.0521	0.0981
σ_{xy}^*	−0.0246	4.5823	−4.6316	−0.0247	1.1981	−1.2474	−0.0238	0.0243	−0.0722
Exact solution[22]									
σ_{xy}^*	0.0258	−9.8794	9.9311	0.0238	−2.017	2.0646	0.0230	−0.0527	0.0987
σ_{xy}^*	−0.0276	4.9764	−5.0316	−0.0248	1.1987	−1.2482	−0.0238	0.0247	−0.0723

[a]Where $u^*=\bar{u}(0, b/2, \pm h/2)$, $w^*=\bar{w}(a/2, b/2, 0)$, $\sigma_x^*=\bar{\sigma}_x(a/2, b/2, \pm h/2)$, $\sigma_y^*=\bar{\sigma}_y(a/2, b/2, \pm h/6)$, and $\sigma_{xy}^*=\bar{\sigma}_{xy}(0, 0, \pm h/2)$.

Table 8 Response of symmetric cross-ply square substrates (0/90/0) under uniformly distributed mechanical load with and without spatially applied uniformly distributed voltage to the PFRC layer

	$s=10$			$s=20$			$s=100$		
Parameter[a]	$V=0$	$V=100$	$V=-100$	$V=0$	$V=100$	$V=-100$	$V=0$	$V=100$	$V=-100$
u^*	0.0092	−4.8115	4.8300	0.0096	−1.2062	1.2254	0.0097	−0.0408	0.0602
	−0.0098	1.7756	−1.7952	−0.0101	0.4475	−0.4678	−0.0102	0.0101	−0.0305
w^*	−0.9513	166.07	−167.97	−0.7044	42.851	−44.259	−0.6236	1.1434	−2.3907
σ_x^*	−0.7343	244.30	−245.77	−0.7622	61.935	−63.459	−0.7661	1.7896	−3.3218
	0.7779	−89.90	91.460	0.8054	−23.397	25.008	0.8088	−0.2098	1.8275
σ_y^*	−0.2726	45.066	−45.611	−0.1938	11.379	−11.767	−0.1702	0.2817	−0.6220
	0.3013	−63.894	64.497	0.2173	−16.127	16.561	0.1921	−0.4495	0.8337
σ_{xy}^*	0.0460	−27.936	28.028	0.0409	−6.5615	6.6433	0.0381	−0.1905	0.2668
	−0.0481	11.718	−11.814	−0.0428	2.4766	−2.5622	−0.0400	−0.2317	−0.1032

[a]Where $u^*=\bar{u}(0, b/2, \pm h/2)$, $w^*=\bar{w}(a/2, b/2, 0)$, $\sigma_x^*=\bar{\sigma}_x(a/2, b/2, \pm h/2)$, $\sigma_y^*=\bar{\sigma}_y(a/2, b/2, \pm h/6)$, and $\sigma_{xy}^*=\bar{\sigma}_{xy}(0, 0, \pm h/2)$.

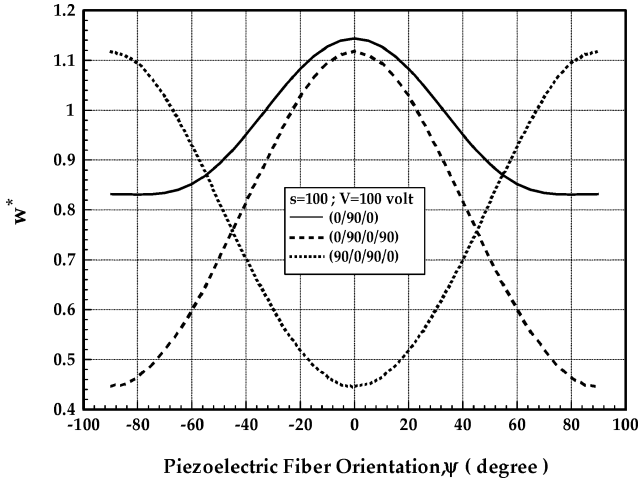

Fig. 3 Variation of center deflection in cross-ply laminates with the piezoelectric fiber angle ψ in the PFRC layer.

where coupling of bending and extensional deformation occurs, the response is highly sensitive to the variation of ψ with respect to the laminate coordinate system. If the top layer of the antisymmetric cross-ply substrate with fiber orientation angle of 90 deg is in contact with the PFRC layer, the actuation capability of the PFRC layer becomes maximum when $\psi=0$ deg and vice versa, as shown in Fig. 3. This indicates that, in the case of an active control system, when the lamination scheme of the overall plate becomes symmetric while the substrate is an antisymmetric cross-ply plate, the control authority of the PFRC layer will be maximum. Similar characteristics of the PFRC layer can also be observed for antisymmetric angle-ply substrate plates as shown in Fig. 4. To investigate the effect of variation of ψ on the response of the substrate where coupling of extensional and in-plane shear deformations occurs, a substrate with only one generally orthotropic layer is considered, and the response for axial displacement u has been studied. Figure 5 shows this response, and it may be observed that the control authority of the PFRC layer is also sensitive to this coupling and becomes maximum when the fiber orientation in the PFRC layer is 0 deg ($\psi=0$ deg).

Finally, the variation of normal stress σ_x across the thickness of the substrates due to the combined action of the spatially uniform

Table 9 Response of antisymmetric cross-ply square substrates (0/90/0/90) under uniformly distributed mechanical load with and without spatially applied uniformly distributed voltage to the PFRC layer

	$s = 10$			$s = 20$			$s = 100$		
Parameter[a]	$V = 0$	$V = 100$	$V = -100$	$V = 0$	$V = 100$	$V = -100$	$V = 0$	$V = 100$	$V = -100$
u^*	0.0014	−7.1797	7.2084	0.0015	−1.6807	1.7098	0.0146	−0.0542	0.0834
	−0.0095	1.7756	−1.7952	−0.0096	0.4497	−0.4690	−0.0097	0.0097	−0.0290
w^*	−0.9889	182.26	−184.24	−0.8070	45.683	−47.297	−0.7474	1.1183	−2.6130
σ_x^*	−0.0505	13.390	−13.491	−0.0510	3.0174	−3.1194	−0.0509	0.0675	−0.1692
	0.7308	−68.019	69.481	0.7407	−10.056	11.538	0.7390	−0.3757	1.1022
σ_y^*	−0.0158	3.6937	−3.7254	−0.0159	0.9875	−1.019	−0.0158	0.0244	−0.0559
	0.6861	−135.48	136.85	0.6823	−41.768	43.132	0.6769	−1.078	2.4318
σ_{xy}^*	0.0431	−34.827	34.913	0.0418	−7.4606	7.5443	0.0411	−0.1999	0.2820
	−0.0450	14.477	−14.567	−0.0436	2.9682	−3.0555	−0.0427	−0.0379	−0.1234

[a]Where $u^* = \bar{u}(0, b/2, \pm h/2)$, $w^* = \bar{w}(a/2, b/2, 0)$, $\sigma_x^* = \bar{\sigma}_x(a/2, b/2, \pm h/2)$, $\sigma_y^* = \bar{\sigma}_y(a/2, b/2, \pm h/6)$, and $\sigma_{xy}^* = \bar{\sigma}_{xy}(0, 0, \pm h/2)$.

Table 10 Response of antisymmetric angle-ply square substrates (−45/45/−45/45) under uniformly distributed mechanical load with and without spatially applied uniformly distributed voltage to the PFRC layer

	$s = 10$			$s = 20$			$s = 100$		
Parameter[a]	$V = 0$	$V = 100$	$V = -100$	$V = 0$	$V = 100$	$V = -100$	$V = 0$	$V = 100$	$V = -100$
u^*	±0.0073	∓3.8935	±3.9081	±0.0072	∓0.8169	±0.8313	±0.0072	∓0.0238	±0.0381
w^*	−0.6664	81.398	−82.730	−0.4847	20.323	−21.292	−0.4266	0.4133	−1.2664
σ_x^*	−0.1950	21.472	−21.862	−0.1979	5.5141	−5.9098	−0.2003	0.0524	−0.4530
	0.1965	−17.825	18.218	0.2001	−4.6504	5.0505	0.2024	−0.0242	0.4290
σ_y^*	−0.1726	19.994	−20.340	−0.1752	5.4029	−5.7532	−0.1768	0.0556	−0.4092
	0.1764	−17.150	17.503	0.1789	−4.9741	5.3320	0.1812	−0.0434	0.4058
σ_{xy}^*	±0.2451	∓104.39	±104.88	±0.2519	∓28.324	±28.828	±0.2547	∓0.8569	±1.3664

[a]Where $u^* = \bar{u}(0, b/2, \pm h/2)$, $w^* = \bar{w}(a/2, b/2, 0)$, $\sigma_x^* = \bar{\sigma}_x(a/2, b/2, \pm h/2)$, $\sigma_y^* = \bar{\sigma}_y(a/2, b/2, \pm h/6)$, and $\sigma_{xy}^* = \bar{\sigma}_{xy}(0, 0, \pm h/2)$.

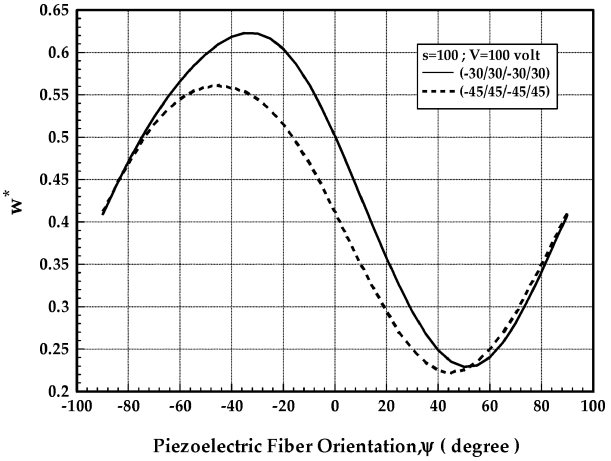

Fig. 4 Variation of center deflection in angle-ply laminates with the piezoelectric fiber angle ψ in the PFRC layer.

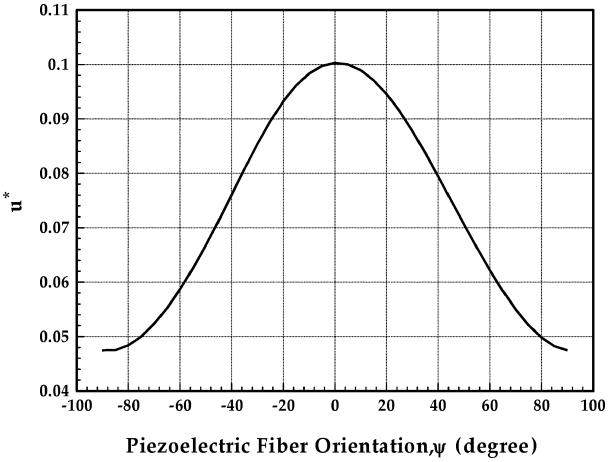

Fig. 5 Variation of center deflection in a single-layered angle-ply substrate ($\theta_1 = 45$ deg) with the piezoelectric fiber angle ψ in the PFRC layer: $s = 100$ and $V = 100$ V.

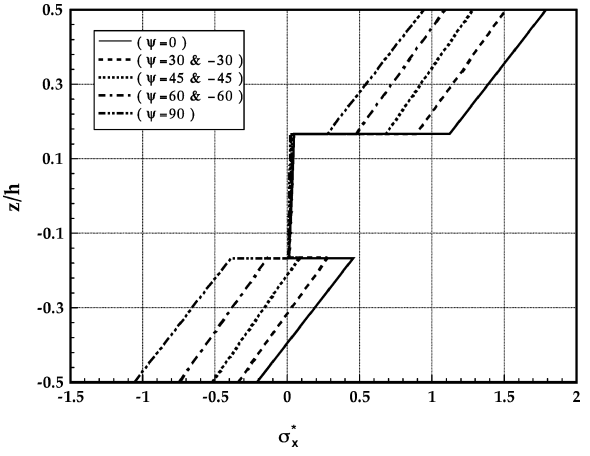

Fig. 6 Distribution of in-plane normal stress σ_x^* across the thickness of thin ($s = 100$) symmetric cross-ply (0/90/0) substrate for different fiber orientation ψ in the activated $V = 100$ V PFRC layer.

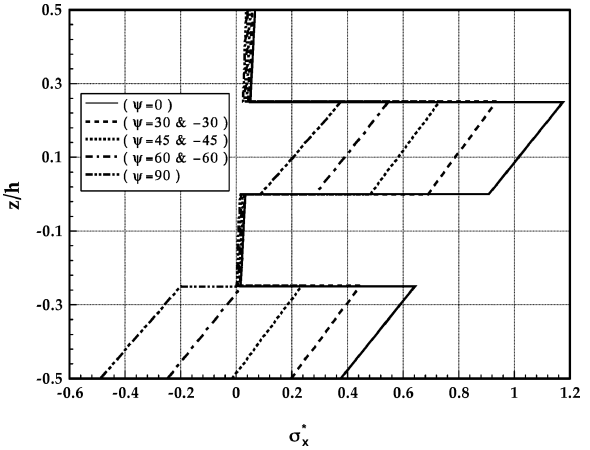

Fig. 7 Distribution of in-plane normal stress σ_x^* across the thickness of thin ($s = 100$) antisymmetric cross-ply (0/90/0/90) substrate for different fiber orientation ψ in the activated $V = 100$ V PFRC layer.

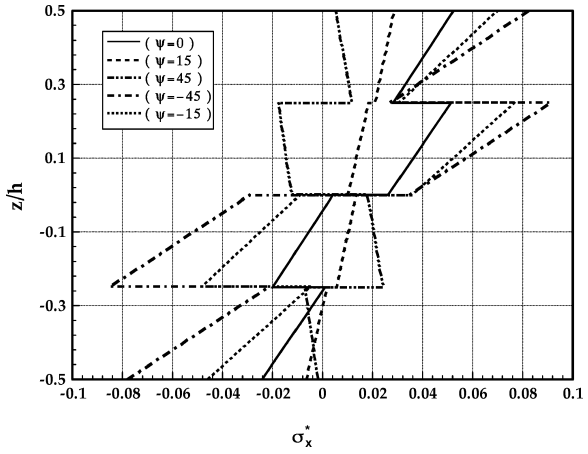

Fig. 8 Distribution of in-plane normal stress σ_x^* across the thickness of thin ($s = 100$) antisymmetric angle-ply ($-45/45/-45/45$) substrate for different fiber orientation ψ in the activated $V = 100$ V PFRC layer.

electric potential on the surface of the PFRC layer and the applied mechanical load ($f_0 = -40$ N/m^2) is shown in Figs. 6, 7, and 8 for thin ($s = 100$) symmetric cross-ply (0/90/0), anti-symmetric cross-ply (0/90/0/90), and antisymmetric angle-ply substrates ($-45/45/-45/45$), respectively. Note from Figs. 6–8 that the distribution of normal stress σ_x in each layer of the substrates has been affected by the activated PFRC layer. In the case of cross-ply substrates, the influence of fiber orientation ψ in the PFRC layer on the actuation of substrate layers does not depend on the sign of the orientation angle ψ, whereas it is sign sensitive in the case of angle-ply substrates. Note that this phenomenon has also been shown in Figs. 3 and 4. When compared with Figs. 3 and 4, Figs. 6–8 also indicate that the fiber angle ψ in the PFRC layer for which the normal stress σ_x is maximum or minimum is same as that for which the center deflection is maximum or minimum.

Conclusions

This paper is concerned with the development of an FEM for assessing the performance of a layer of PFRC material as a distributed actuator for laminated composite plates. Both symmetric and antisymmetric cross-ply and angle-ply laminated substrates are considered. The FEM is based on the FSDT. The results obtained by this model when compared with the exact solutions indicate excellent agreement for thin substrates, whereas the results differ from the exact solutions with marginal error in case of thick substrates. This can be because, in case of thick substrates, consideration of high-order shear deformation has not been employed. Because the practical structures are in general thin structures, the present FEM can be efficiently used for studying the performance of the PFRC layer as a distributed actuator for smart laminated composite plates. The fiber orientation in the PFRC layer plays significant role in actuating the laminated substrates. For antisymmetric laminated substrates, if the fiber orientation in the PFRC layer is such that the stacking sequence of the overall plate (substrate with PFRC layer) becomes symmetric with respect to the middle layer, then the control authority of the PFRC layer becomes maximum. The control authority of the PFRC layer is independent of the sign of the fiber orientation angle in the PFRC layer for cross-ply substrates, whereas it is dependent on the sign of this fiber orientation for angle-ply substrates.

References

[1]Bailey, T., and Hubbard, J. E., "Distributed Piezoelectric Polymer Active Vibration Control of a Cantilever Beam," *Journal of Guidance, Control, and Dynamics*, Vol. 8, No. 5, 1985, pp. 605–611.

[2]Crawley, E. F., and Luis, J. D., "Use of Piezoelectric Actuators as Elements of Intelligent Structures," *AIAA Journal*, Vol. 25, No. 10, 1987, pp. 1373–1385.

[3]Baz, A., and Poh, S., "Performance of an Active Control System with Piezoelectric Actuators," *Journal of Sound and Vibration*, Vol. 126, No. 2, 1988, pp. 327–343.

[4]Tzou, H. S., and Tseng, C. I., "Distributed Piezoelectric Sensor/Actuator Design for Dynamic Measurement/Control of Distributed Parameter Systems: A Piezoelectric Finite Element Approach," *Journal of Sound and Vibration*, Vol. 138, No. 1, 1990, pp. 17–34.

[5]Lee, C. K., Chiang, W. W., and Sulivan, O., "Piezoelectric Modal Sensor/Actuator Pairs for Critical Active Damping Vibration Control," *Journal of the Acoustical Society of America*, Vol. 90, No. 1, 1991, pp. 374–384.

[6]Hanagud, S., Obal, M. W., and Calise, A. J., "Optimal Vibration Control by the Use of Piezoceramic Sensors and Actuators," *Journal of Guidance, Control, and Dynamics*, Vol. 15, No. 5, 1992, pp. 1199–1206.

[7]Ray, M. C., Bhattacharyya, R., and Samanta, B., "Exact Solutions for Static Analysis of Intelligent Structures," *AIAA Journal*, Vol. 31, No. 9, 1993, pp. 1684–1691.

[8]Devasia, S., Tesfay, M., Paden, B., and Bayo, E. A. J., "Piezoelectric Actuator Design for Vibration Suppression: Placement and Sizing," *Journal of Guidance, Control, and Dynamics*, Vol. 16, 1993, pp. 859–864.

[9]Gu, Y., Clark, R. L., and Fuller, C. R., "Experiments on Active Control of Plate Vibration Using Piezoelectric Actuators and Polyvinylidyne Fluoride (PVDF) Modal Sensors," *Journal of Vibration and Acoustics*, Vol. 116, 1994, pp. 303–308.

[10]Zhou, R. C., Lai, Z., Xue, D. Y., Huang, J. K., and Mei, C., "Suppression of Nonlinear Panel Flutter with Piezoelectric Actuators Using Finite Element Method," *AIAA Journal*, Vol. 6, 1995, pp. 1098–1105.

[11]Samanta, B., Ray, M. C., and Bhattacharyya, R., "Finite Element Model for Active Control of Intelligent Structures," *AIAA Journal*, Vol. 34, No. 9, 1996, pp. 1885–1893.

[12]Baz, A., and Poh, S., "Optimal Vibration Control with Modal Positive Position Feedback," *Optimal Control Applications and Methods*, Vol. 17, 1996, pp. 141–149.

[13]Ray, M. C., "Optimal Control of Laminated Plates with Piezoelectric Sensor and Actuator Layers," *AIAA Journal*, Vol. 36, No. 12, 1998, pp. 2204–2208.

[14]Agarwal, B. N., and Treanor, K. E., "Shape Control of a Beam Using Piezoelectric Actuators," *Smart Materials and Structures*, Vol. 8, 1999, pp. 729–740.

[15]Stöbener, U., and Gaul, L., "Modal Vibration Control for PVDF Coated Plates," *Journal of Intelligent Material Systems and Structures*, Vol. 11, No. 4, 2000, pp. 283–293.

[16]Dong, S., and Tong, L., "Vibration Control of Plates Using Discretely Distributed Piezoelectric Quasi-Modal Actuators/Sensors," *AIAA Journal*, Vol. 39, 2001, pp. 1766–1772.

[17]Ray, M. C., "Optimal Control of Laminated Shells with Piezoelectric Sensor and Actuator Layers," *AIAA Journal*, Vol. 41, No. 6, 2003, pp. 1151–1157.

[18]Varadan, V. V., Kim, J., and Varadan, V. K., "Optimal Placement of Piezoelectric Actuators for Active Noise Control," *AIAA Journal*, Vol. 35, 1997, pp. 526–533.

[19]Fuller, C. R., Synder, S. D., Hansen, C. H., and Silcox, R. J., "Active Control of Interior Noise in Model Aircraft Fuselages Using Piezoceramic Actuators," *AIAA Journal*, Vol. 30, No. 11, 1992, pp. 2613–2617.

[20]Steven, A. L., Steven, G., and Don, L., "Active Structural Acoustic Control of a Launch Vehicle Fairing Using Monolithic Piezoceramic Actuators," *Journal of Intelligent Material Systems and Structures*, Vol. 12, 2001, pp. 795–806.

[21]Mallik, N., and Ray, M. C., "Effective Coefficients of Piezoelectric Fiber Reinforced Composites," *AIAA Journal*, Vol. 41, No. 4, 2003, pp. 704–710.

[22]Mallik, N., and Ray, M. C., "Exact Solutions for Static Analysis of Smart Structures with a Layer of Piezoelectric Fiber Reinforced Composites," *International Journal of Solids and Structures* (submitted for publication).

[23]Reddy, J. N., *Mechanics of Laminated Composite Plates Theory and Analysis*, CRC Press, Boca Raton, FL, 1996.

M. Ahmadian
Associate Editor